

Quantum dynamics in a camel-back potential of a dc SQUID

E. Hoskinson¹, F. Lecocq¹, N. Didier², A. Fay¹, F. W. J. Hekking², W. Guichard¹ and O. Buisson¹
¹*Institut Néel, C.N.R.S.- Université Joseph Fourier, BP 166, 38042 Grenoble-cedex 9, France and*
²*LPMMC, C.N.R.S.- Université Joseph Fourier, BP 166, 38042 Grenoble-cedex 9, France*

R. Dolata, B. Mackrodt and A. B. Zorin

Physikalisch-Technische Bundesanstalt, Bundesallee 100, 38116 Braunschweig, Germany

(Dated: August 11, 2024)

We investigate the quantum dynamics of a quadratic-quartic anharmonic oscillator formed by a potential well between two potential barriers. We realize this novel potential shape with a superconducting circuit comprised of a loop interrupted by two Josephson junctions, with near-zero current bias and flux bias near half a flux quantum. We investigate escape out of the central well, which can occur via tunneling through either of the two barriers, and find good agreement with a generalized double-path macroscopic quantum tunneling theory. We also demonstrate that this system exhibits an “optimal line” in current and flux bias space along which the oscillator, which can be operated as a phase qubit, is insensitive to decoherence due to low-frequency current fluctuations.

Superconducting devices, based on the nonlinearity of the Josephson junction (JJ), exhibit a wide variety of quantum phenomena. During the last decade, inspired by Macroscopic Quantum Tunneling (MQT) studies [1], quantum dynamics of the current biased JJ, dc SQUID and the rf SQUID phase qubit have been extensively studied [2, 3, 4, 5, 6]. In each of these devices, the dynamics can be described as those of a quantum particle in a quadratic-cubic potential. The flux qubit system [7], realized by three or four JJs in a loop, is described by a double well potential. Here we propose to study a new potential shape called hereafter a “camel-back” double barrier potential, shown in Fig. 1c. This potential is obtained using the dc SQUID circuit shown in Fig. 1a in a new way. The characteristics of the camel-back potential, including depth and relative barrier height, are controlled by the SQUID current bias I_b and flux bias Φ_{ext} . There is a special line we call the “optimal line” in these two bias parameters at which the barrier heights are equal and anharmonicity is quartic. Because of the symmetry of the potential, the system can escape from the central well via tunneling through either of the two barriers to an adjacent deeper well. We investigate this double path escape and analyse it using MQT theory. When the depth of the central well is adjusted so that the escape rate is negligible but anharmonicity is significant, the two lowest energy levels $|0\rangle$ and $|1\rangle$ constitute a phase qubit. We show that this qubit is insensitive to dephasing due to current bias fluctuations on the optimal line.

A dc SQUID circuit has two degrees of freedom corresponding to the phase differences ϕ_1 and ϕ_2 across its two JJs. The dynamics are analogous to those of a particle of mass $m = 2C(\Phi_0/2\pi)^2$ in the 2-D potential [8, 9]

$$U(x, y) = U_0[-\cos x \cos y - sx + b(y - y_b)^2 - \alpha \sin x \sin y - \eta sy]. \quad (1)$$

Here $x = (\phi_1 + \phi_2)/2$ and $y = (\phi_1 - \phi_2)/2$. Fixed

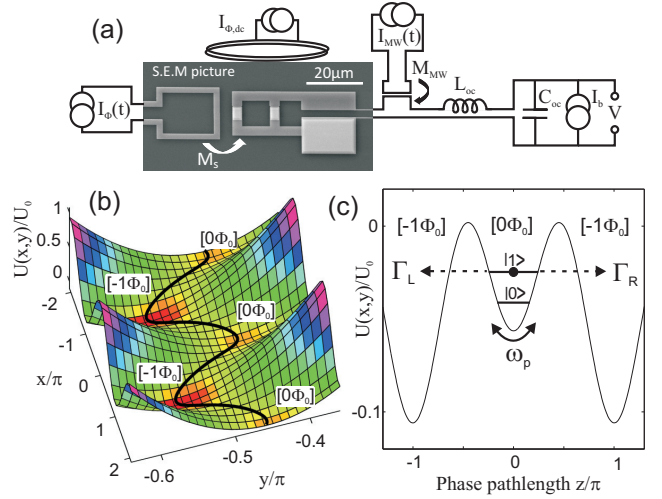


FIG. 1: Schematic of experimental setup and camel-back potential. (a) Circuit layout. (b) Full 2-D potential for $b = 3.05$, $\eta = 0.72$, $\alpha = 0$, $\Phi_{\text{ext}} = -0.508\Phi_0$, $I_b = 0$, showing the families of minima associated with the $[0\Phi_0]$ and $[-1\Phi_0]$ fluxoid states. The black line follows the minimum energy path. (c) Potential along the minimum energy path, parameterized by the path length.

for a given sample are the Josephson energy $U_0 = (I_{c1} + I_{c2})\Phi_0/2\pi$, the junction to loop inductance ratio $b = \Phi_0/2\pi LI_c$, the critical current asymmetry $\alpha = (I_{c2} - I_{c1})/2I_c$, and the loop inductance asymmetry $\eta = (L_2 - L_1)/L$. Here $I_c = I_{c1} + I_{c2}$, I_{c1} and I_{c2} are the critical currents of the two junctions, L_1 and L_2 are the geometric inductances of the two arms of the SQUID loop, $L = L_1 + L_2$, C is the capacitance of each junction, and $\Phi_0 = h/2e$ is the quantum of flux. The external control parameters I_b and Φ_{ext} enter into the potential through $y_b = \pi\Phi_{\text{ext}}/\Phi_0$ and $s = I_b/I_c$. For our sample, $I_c = 11.22 \mu\text{A}$, $C = 250.3 \text{ fF}$, $b = 3.05$, $\eta = 0.72$, and $\alpha = 0.0072$.

The first term in $U(x, y)$, due to the junctions, de-

scribes a 2-D periodic array of minima and maxima. This array can be tilted in the x -direction with an applied current bias. Magnetic field energy associated with circulating current gives rise to the parabolic term in the y -direction, the minimum of which is shifted by the external flux.

Stable, stationary states of the system correspond to minima of $U(x, y)$. There can exist one, two, or more minima families corresponding to distinct fluxoid states $[n\Phi_0]$. For each, when s exceeds a flux dependent critical value $s_c[n\Phi_0](y_b)$, the related local minima disappear. For small values of b , the parabolic term in $U(x, y)$ is shallow, and there can be many fluxoid states. For $b \gg 1/\pi$, as in our case, the parabolic term is steep and there is only one stable fluxoid state except in a small region around $\Phi_{\text{ext}}/\Phi_0 = 0.5 \pmod{1}$, $I_b \approx 0$ where there are two states with opposite circulating current. Hereafter we will be focusing on this region.

In general, dynamics is described by 2-D motion in the potential. In our case, the particle moves through a valley in which the curvature is much larger in one direction (~ 100 GHz) than the other (10-20 GHz). To a good approximation therefore, motion is one dimensional along the path of minimum curvature which connects minima and saddle points. We parametrize this path with the phase length z (see black line in Fig. 1b). $U(z)$ in Fig. 1c depicts the ‘‘camel-back’’ potential shape we are investigating. In a typical experiment, the system is initialized in the central well, which corresponds to the $[0\Phi_0]$ fluxoid state. The deeper wells on either side of the central well both correspond to the $[-1\Phi_0]$ fluxoid state. Starting from the central well, the system can escape via tunneling through the barriers in either of the two physically distinct directions to the $[-1\Phi_0]$ fluxoid state.

In the perfectly symmetric case, the potential near the central minimum will be harmonic with a quartic perturbation. More generally, the Hamiltonian for small oscillations in $U(z)$ is

$$H = \frac{1}{2} \hbar \omega_p (\hat{P}^2 + \hat{Z}^2) - \sigma \hbar \omega_p \hat{Z}^3 - \delta \hbar \omega_p \hat{Z}^4. \quad (2)$$

Here ω_p is the zero amplitude oscillation frequency in the direction of minimum curvature, and $\hat{Z} = z\sqrt{m\omega_p/\hbar}$ and $\hat{P} = p/\sqrt{\hbar\omega_p m}$ are the reduced position and corresponding momentum operators. Treating the anharmonic terms as perturbations, to second order the transition energy between levels $n-1$ and n is $\hbar\omega_{n-1,n} = \hbar\omega(1-n\Lambda)$, where the anharmonicity is $\Lambda = \frac{15}{2}\sigma^2 + 3\delta$ [10]. We have calculated the escape probability for the camel-back potential with a double escape path in the quantum limit using the instanton formalism [11]. For a duration Δt , it reads $P_{\text{esc}}(I_b, \Phi_{\text{ext}}) = 1 - e^{-(\Gamma_R + \Gamma_L)\Delta t}$, where $\Gamma_{R,L} = A_{R,L}\omega\sqrt{N_{R,L}}\exp[-B_{R,L}N_{R,L}]$. Here R and L refer to the right and left barriers. $N_{R,L} = \Delta U_{R,L}/\hbar\omega$ are the normalized barrier heights. The general expression of the coefficients $A_{R,L}$, and $B_{R,L}$ depends on the poten-

tial shape. In the symmetric case where $\sigma(I_b, \Phi_{\text{ext}}) = 0$, the potential is quadratic-quartic, $A_{R,L} = 2^{\frac{5}{2}}\pi^{-\frac{1}{2}}$ and $B_{R,L} = 16/3$. Far from this symmetric line the potential is quadratic-cubic, the escape rate through one barrier is dominant (*e.g.* $\Gamma_L = 0$), and we retrieve the standard MQT situation ($\delta = 0$): $A_R = 6^{\frac{3}{2}}\pi^{-\frac{1}{2}}$ and $B_R = 36/5$ [1].

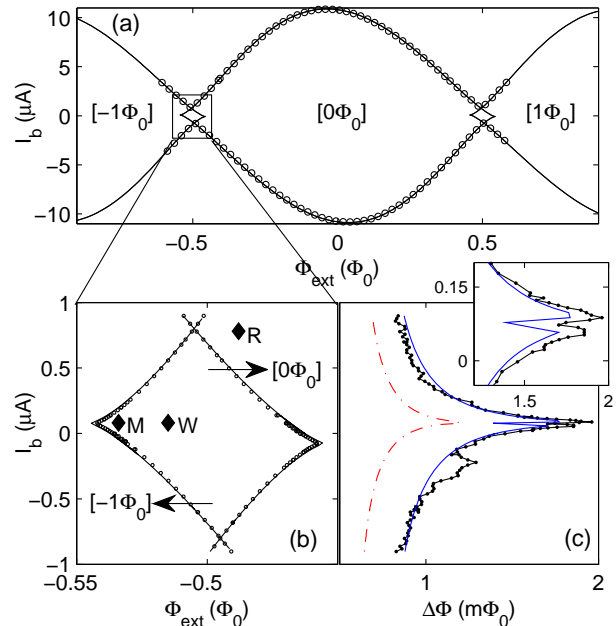


FIG. 2: Escape from the ground state. (a) Critical lines of three neighboring fluxoid states, measured (symbols), and standard MQT theory fit (lines), denoting $I_{50\%}$, the amplitude of a $60 \mu\text{s}$ I_b pulse that yields $P_{\text{esc}} = 50\%$ to the voltage state of the SQUID. (b) Critical lines representing 50% escape out of fluxoid states $[0\Phi_0]$ and $[-1\Phi_0]$ in the region around $\Phi_{\text{ext}} = -\Phi_0/2$ due to a 100 ns flux pulse, measured (symbols), and the generalized MQT theory fit (lines). The $[0\Phi_0]$ and $[-1\Phi_0]$ fluxoid states are both stable in the central region enclosed by the critical lines. Escape is either to the SQUID voltage state ($I_b > 0.8 \mu\text{A}$) or to the adjacent fluxoid state ($I_b < 0.8 \mu\text{A}$). The points W, M, and R indicate the Working point, quantum Measurement point and Readout point for a typical camel-back potential phase qubit experiment. (c) Width of ground-state escape $\Delta\Phi$: measurements (points+lines), and generalized MQT theory with (solid line) and without (dashed line) 9 nA RMS low-frequency current noise. The location of the dip near the maximum $\Delta\Phi$ corresponds to the point where symmetry leads to a reduction in sensitivity to noise.

A schematic of our experimental setup is shown in Fig. 1a. Our sample was fabricated at PTB using a Nb/ AlO_x /Nb trilayer process with SiO_2 dielectric and a critical current density of 300 A/cm^2 [12]. The $5 \mu\text{m}^2$ junctions are embedded in a square loop with inner size $10 \times 10 \mu\text{m}^2$. An off-chip coil provides a dc flux bias. Current bias and voltage leads, heavily filtered at various stages of the cryostat [13], connect at the right of the

SQUID. Fast flux pulses are inductively coupled via the on-chip loop to the left of the SQUID. Microwave (MW) excitation is applied via an on-chip loop which couples inductively to the current bias leads. The MW excitation must be in *current*, rather than flux, because for the symmetric camel potential, small amplitude oscillations occur for the most part in the x direction, and therefore must be excited via the $-sx$ term in $U(x, y)$. The fast flux and MW excitation lines are $50\ \Omega$ coaxial with -20 dB attenuators at 1 K and base temperature. The SQUID chip is enclosed in a small copper box thermally anchored to the mixing chamber of a dilution refrigerator with a base temperature of 30 mK. The cryostat is surrounded by a superconducting Pb shield, inside a μ -metal shield, inside a soft iron shield.

Fig. 2a shows the switching current $I_{50\%} \simeq I_{cSc}[n\Phi_0](y_b)$ as a function of flux for the $[-1\Phi_0]$, $[0\Phi_0]$, and $[1\Phi_0]$ fluxoid states. The interior of each curve is the region where the corresponding flux state is stable. The measurements shown in Fig. 2a were obtained with a standard technique in which I_b pulses of varying amplitude are applied and a dc voltage detected across the SQUID when it switches to its voltage state. With this scheme, however, there is no direct indication of multiply stable flux states. In Fig. 2b we use a novel technique to measure the overlapping critical lines of $[0\Phi_0]$ and $[-1\Phi_0]$ flux states close to $\Phi_{\text{ext}}/\Phi_0 = -0.5$. These two interior critical lines represent transitions between the two flux states, rather than transitions to the voltage state, which is why the standard technique does not detect them.

Our novel escape measurement method proceeds as follows. First, if necessary, the system is initialized in the desired flux state with an adiabatic pulse on the fast flux line. I_b is brought to its working point value. A flux pulse $\delta\Phi$ is applied via the fast line for a fixed nanosecond-scale duration, bringing the total externally applied flux to a “measurement point” close to the critical line. This has the effect of reducing the heights $\Delta U_{R,L}$ of the two potential barriers. P_{esc} via tunneling from the central well through the barriers to the neighboring deeper wells is thereby greatly increased. The system is brought back to a flux at which both fluxoid states are stable. The fluxoid state is then read out via a slow ($\sim 10\ \mu\text{s}$) I_b pulse. This I_b pulse brings the system outside the critical line of fluxoid state $[-1\Phi_0]$ but well within that of $[0\Phi_0]$. If the system is in state $[-1\Phi_0]$, it will switch, producing a voltage which is detected. If it is in state $[0\Phi_0]$, it will not switch. We achieve a one-shot discrimination between flux states of 100% with this readout. The process is completed by bringing I_b to zero and waiting 100 μs for the heat generated by a switching event to dissipate before repeating. Multiple repetitions, at a rate of about 5 kHz, yield P_{esc} .

The overlapping $P_{\text{esc}} = 50\%$ critical lines separating the $[-1\Phi_0]$ and $[0\Phi_0]$ fluxoid states are plotted in Fig. 2b. Each ends in a cusp at the extreme value of flux where

the corresponding fluxoid state is stable. These cusps occur at a non-zero current bias $I_b^{\text{cusp}} = \pm\alpha I_c = \pm 81\ \text{nA}$ due to the critical current asymmetry α . The horizontal separation of the cusps scales precisely with $1/b$. Our generalized MQT theory is accurately able to reproduce the measured data of fig 2b. Of the parameters that go into this theory, b and α are treated as free parameters in this fit, I_c and η are determined by the fit in Fig. 2a and C is determined by a fit to spectroscopic data.

Along the critical line of a given fluxoid state, for I_b above or below the value I_b^{cusp} , the potential is tilted to the right or to the left, and escape occurs preferentially in that direction. At I_b^{cusp} , the camel potential is symmetric around the minima ($\sigma = 0$), the two potential barrier heights are equal, and escape occurs with equal probability in either direction. The cusps in Fig. 2b correspond therefore to a double-path escape.

The width of the escape process contains additional information about the dependence of the potential on the bias parameters, and on fluctuations in the bias parameters [14]. In Fig. 2c, we plot the width $\Delta\Phi = |\Phi_{80\%} - \Phi_{20\%}|$, as a function of I_b . This plot peaks around I_b^{cusp} , except that at this point there is a sharp dip (see insert). This behavior is explained by double-path MQT escape if we include low frequency current fluctuations. In this circuit thermal fluctuations are expected in I_b , which we estimate to be on the order of 10 nA RMS by the equipartition theorem $\frac{1}{2}kT = \frac{1}{2}LI_{\text{RMS}}^2$, where k is Boltzmann’s constant, $T \simeq 40\ \text{mK}$ is the circuit temperature, and $L \simeq 10\ \text{nH}$ is the series isolating inductance. Because of this noise, the escape probability is averaged: $\langle P_{\text{esc}}(I_b, \Phi_{\text{ext}}) \rangle$. The angle brackets represent a convolution with the probability distribution of I_b , which we assume to be Gaussian with standard deviation I_{RMS} . As shown in Fig. 2c, the addition of $I_{\text{RMS}} = 9\ \text{nA}$ is accurately able to explain both the increase in the overall width, and the presence of a distinctive dip at I_b^{cusp} which is a result of symmetry in escape direction. The presence of the dip and our ability to reproduce it with MQT theory is a striking confirmation of double path escape and low frequency I_b fluctuations in our sample.

In Fig. 3a and b we investigate the operation of a camel-back potential phase qubit corresponding to the two lowest levels $|0\rangle$ and $|1\rangle$ of the anharmonic central well related to the $[0\Phi_0]$ flux state (see fig 1c). For these measurements we use the same procedure as for the ground-state escape measurements except that before the nanosecond measurement pulse, an adiabatic flux pulse brings the system to the working point flux Φ_W where a MW pulse is applied to the fast current line. At the working point, the barriers are high enough that P_{esc} is negligible. Immediately following the MW pulse we apply a 5 ns pulse which projects the qubit state onto the flux state of the SQUID. This is possible because P_{esc} depends exponentially on the excitation level of the qubit. The amplitude of the measuring flux pulse is tuned such

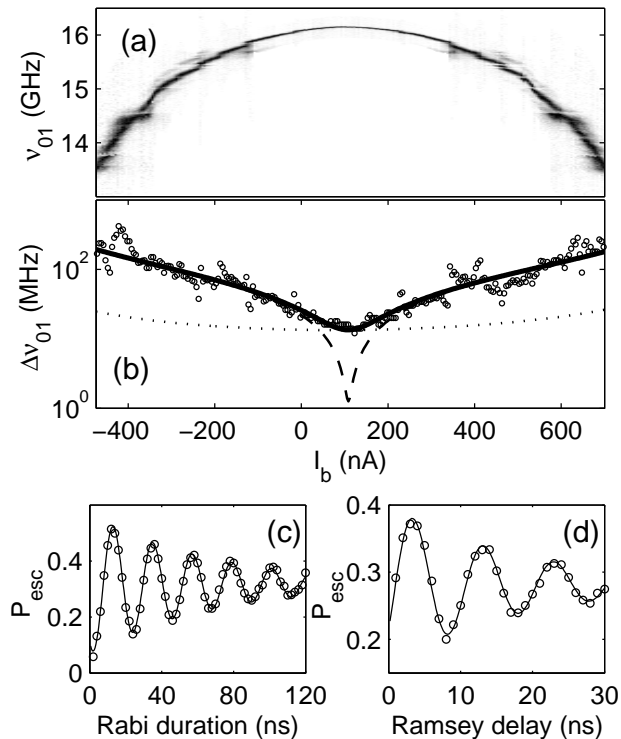


FIG. 3: (a) P_{esc} versus I_b and MW frequency. Dark and bright grayscale correspond to high and small P_{esc} . (b) Width of the resonance on a semi-log scale. The dashed line is the predicted contribution due to 9 nA RMS low-frequency current noise. The dotted line is for $40 \mu\Phi_0$ RMS low-frequency flux noise. The sum of these two contributions, the solid line, accurately reproduces the data (symbols). Rabi (c) and Ramsey (d) oscillations at the optimal line at $I_b = -71$ nA, $\Phi_{\text{ext}}/\Phi_0 = -0.468$ for the $[-1\Phi_0]$ flux state.

that escape will occur with high probability if the qubit is excited, and low probability if it is not. The measurement pulse transfers the quantum states $|0\rangle$ and $|1\rangle$ of the qubit to the classical fluxoid states $[0\Phi_0]$ and $[-1\Phi_0]$ of the SQUID. Readout of the fluxoid state, which is itself stable, reveals the projected qubit state, and repetition yields P_{esc} .

P_{esc} was measured as a function of MW frequency ν and I_b . Because the MW pulse duration, 800 ns, is much longer than the relaxation time $T_1 \simeq 100$ ns, the system reaches a steady state. A peak in P_{esc} appears when ν matches the qubit transition frequency ν_{01} . Fig. 3a shows ν_{01} as function of I_b . It reaches a maximum at $I_b^{\text{op}}(\Phi_{\text{ext}})$ which corresponds to the camel potential symmetric point. Note that this optimal point is a function of flux, and is terminated by the cusp at the critical line. This data was taken at $\Phi_{\text{ext}} = -0.503\Phi_0$ for the $[0\Phi_0]$ fluxoid state. Apparent in this spectroscopic image are avoided level crossings with what are likely microscopic two-level fluctuators, as first observed by Ref.[3]. We observe on average 20 crossings per GHz. In Fig. 3b, the

spectroscopic width of the ν_{01} transition $\Delta\nu_{01}$ is plotted as a function of I_b . A sharp minimum is observed at $I_b = 108$ nA, corresponding to the flat maximum in ν_{01} .

We find that we can accurately model $\Delta\nu_{01}(I_b)$ with a combination of low-frequency current and flux fluctuations. Because ν_{01} depends on the bias parameters, fluctuations cause ν_{01} to vary from repetition to repetition, smearing out the observed resonance. Assuming a Gaussian fluctuation distribution, the predicted variance in ν_{01} is $(\frac{\Delta\nu_I}{2})^2 = \left(\frac{\partial\nu}{\partial I_b}\right)^2 I_{\text{RMS}}^2 + \frac{1}{2} \left(\frac{\partial^2\nu}{\partial I_b^2}\right)^2 I_{\text{RMS}}^4$, for current fluctuations alone, and $(\frac{\Delta\nu_\Phi}{2})^2 = \left(\frac{\partial\nu}{\partial\Phi_{\text{ext}}}\right)^2 \Phi_{\text{RMS}}^2$ for flux fluctuations alone. Here $\Delta\nu_I$ has been expanded to second order in I_{RMS} since $\frac{\partial\nu}{\partial I_b}$ is zero at the optimal line. In Fig. 3b, the predicted $\Delta\nu_I$ is plotted as a dashed line for $I_{\text{RMS}} = 9$ nA, precisely the same current fluctuation amplitude used in Fig. 2c. The dotted line plots $\Delta\nu_\Phi$ for $\Phi_{\text{RMS}} = 40 \mu\Phi_0$. The solid line is the combined prediction $\Delta\nu = \sqrt{\Delta\nu_I^2 + \Delta\nu_\Phi^2}$. The dashed line is obscured behind the solid line except in a small region around the optimal current. This plot vividly demonstrates the idea of the optimal line: the effects of current bias fluctuations, which accurately account for the spectral width away from the optimal line, are rendered negligible on the optimal line. The residual spectroscopic width, about 10 MHz, can be explained by a flux noise of $40 \mu\Phi_0$ RMS. Since the decoherence time T_2 scales inversely with $\Delta\nu_{01}$, this optimal line is also optimal for qubit operations. Along this line Rabi and Ramsey oscillations (Fig. 3c and d) were measured giving coherence times of $T_{\text{Rabi}} = 67$ ns and $T_{\text{Ramsey}} = 18$ ns for this current sample. The anharmonicity is large enough and the applied power small enough that excitation beyond the first excited state is negligible, as we have verified by the linearity of Rabi frequency versus power. The system is confined to its lowest two levels and can therefore be considered a qubit.

In conclusion, we have studied the quantum dynamics of a novel quadratic-quartic ‘‘camel’’ potential created in a dc SQUID circuit with $I_b \simeq 0$, $\Phi_{\text{ext}} \simeq 0.5\Phi_0$. Ground state escape exhibits critical line cusps and a dip in the escape width versus bias-current. We explain these two effects with a generalized double-path MQT escape theory. Moreover due to the particular potential symmetry, the quantum dynamics is insensitive in first order to current fluctuations along an optimal line $I_b^{\text{op}}(\Phi_{\text{ext}})$. Along this line, the dc SQUID can be used as a phase qubit whose main decoherence sources are residual flux noise and microscopic two-level fluctuators. Future optimization and exploitation of the unique properties of this system will aid in the understanding of decoherence mechanisms in quantum circuits and has the potential to yield a competitive phase qubit.

This work was supported by two ACI programs, by the EuroSQIP and INTAS projects.

-
- [1] *Quantum Tunneling in Condensed Media*, Modern Problems in Condensed Matter Sciences, Vol. 34, edited by Yu. Kagan and A. J. Leggett (Elsevier Science Publishers, 1992).
- [2] J. M. Martinis, S. Nam, J. Aumentado, and C. Urbina, Phys. Rev. Lett. **89**, 117901 (2002).
- [3] K.B. Cooper *et al.*, Phys. Rev. Lett. **93**, 180401 (2004).
- [4] J. Claudon, F. Balestro, F. W. J. Hekking, and O. Buisson, Phys. Rev. Lett. **93**, 187003 (2004).
- [5] J. Lisenfeld, A. Lukashenko, M. Ansmann, J. M. Martinis, and A. V. Ustinov, Phys. Rev. Lett **99**, 170504 (2007).
- [6] S. K. Dutta *et al.*, arXiv 0806.4711 (2008).
- [7] I. Chiorescu, Y. Nakamura, C. J. P. M. Harmans, and J. E. Mooij, Science **299**, 1869 (2003).
- [8] C. D. Tesche and J. Clarke, J. Low Temp. Phys. **29**, 301 (1977).
- [9] V. Lefevre-Seguin, E. Turlot, C. Urbina, D. Esteve, and M. H. Devoret, Phys. Rev. B **46**, 5507 (1992).
- [10] L. D. Landau and L. M. Lifshitz, *Quantum Mechanics: Non-Relativistic Theory* (Course of Theoretical Physics, Volume 3), (3ed., Pergamon, 1991).
- [11] C. G. Callan and S. Coleman, Phys. Rev. D **16**, 1762 (1977).
- [12] R. Dolata, H. Scherer, A. B. Zorin, and J. Niemeyer, J. Appl. Phys. **97**, 054501 (2005).
- [13] A. Fay, PhD thesis, Université Joseph Fourier, 2008.
- [14] J. Claudon, A. Fay, E. Hoskinson, and O. Buisson, Phys. Rev. B **76**, 024508 (2007).